Optics and Lasers in Engineering 48 (2010) 512–517

Contents lists available at ScienceDirect

Optics and Lasers in Engineering

journal homepage: www.elsevier.com/locate/optlaseng

Study on microstructure and mechanical properties of 304 stainless steel joints by TIG, laser and laser-TIG hybrid welding

Jun Yan, Ming Gao, Xiaoyan Zeng *

Division of Laser Science and Technology, Wuhan National Laboratory for Optoelectronics, School of Optoelectronics Science and Engineering, Huazhong University of Science and Technology, Wuhan, Hubei 430074, PR China

ARTICLE INFO

Article history:
Received 26 May 2009
Received in revised form
26 July 2009
Accepted 17 August 2009
Available online 26 September 2009

Keywords:
Laser welding
Hybrid welding
304 stainless steel
Mechanical properties

ABSTRACT

This paper investigated the microstructure and mechanical properties of 304 stainless steel joints by tungsten inert gas (TIG) welding, laser welding and laser-TIG hybrid welding. The X-ray diffraction was used to analyze the phase composition, while the microscopy was conducted to study the microstructure characters of joints. Finally, tensile tests were performed and the fracture surfaces were analyzed. The results showed that the joint by laser welding had highest tensile strength and smallest dendrite size in all joints, while the joint by TIG welding had lowest tensile strength, biggest dendrite size. Furthermore, transition zone and heat affected zone can be observed in the joint of TIG welding. The fractograph observation showed that the TIG welding joint existed as cup–cone shaped fracture, while the laser welding and hybrid welding joints existed as pure-shear fracture. The laser welding and hybrid welding are suitable for welding 304 stainless steel owing to their high welding speed and excellent mechanical properties.

1. Introduction

Austenitic stainless steels have been widely used as nuclear structural materials for reactor coolant piping, valve bodies, and vessel internals because of their excellent mechanical properties. However, welding often leads to low mechanical properties owing to the metallurgical changes such as micro-segregation, precipitation of secondary phases, presence of porosities, solidification cracking, grain growth in the heat affected zone (HAZ) and loss of materials by vaporization [1,2]. Generally speaking, welding is one of the most widely used processes to fabricate stainless steel structures. The conventional arc welding is often sensitive to form the coarse grains and intergranular Cr-rich carbides along the grain boundaries in HAZ, which deteriorates the mechanical properties of the joints [3–5]. As a new fusion welding method, the laser-TIG hybrid welding integrates laser beam and electric arc. Advantages of hybrid process over arc welding and laser welding include higher welding stability, higher melting efficiency and lower power input under the same penetration [6,7]. Up to now, so many people have carried out the study on hybrid welding.

It is well known that the microstructure of 304 stainless steel is mainly composed of austenite (γ-Fe) under the condition of equilibrium solidification. However, during the non-equilibrium rapid solidification condition, the high cooling rate will result in incomplete $\delta \rightarrow \gamma$ transformation and some metastable δ-Fe should be remained unavoidably [8,9]. It is well known that the ferrite-to-austenite ratio depends on the heat-input in the 304 stainless steel welding process. However, for achieving the same penetration, different heat-input should be adopted by the TIG welding, laser welding and laser-TIG hybrid welding methods because of their different heat source characters. Thus, different ferrite-to-austenite ratio should be formed in the fusion zone by the three welding methods. It has been reported that the mechanical properties of stainless steel strongly depend on the microstructure in joints. Thus, carrying out the study on the relationship between microstructure and mechanical properties is needed widely. Berretta [10] had studied the pulsed Nd:YAG laser welding of AISI 304–AISI 420 stainless steels. Anawa [11] optimized the tensile strength of ferritic/austenitic laser-welded components. However, the mechanical properties of austenitic stainless steel welded by laser-TIG hybrid welding have been reported seldom. Especially, the effect of welding methods on mechanical properties of austenitic stainless steel is not investigated comparatively.

In this study, 3 mm thick 304 stainless steel plates were welded by TIG welding, laser welding and laser-TIG hybrid welding, respectively. Characterization of macrostructure, microstructure

* Corresponding author.
E-mail addresses: hustyanjun@163.com (J. Yan), xyzeng@mail.hust.edu.cn (X. Zeng).

0143-8166/$ - see front matter Crown Copyright © 2009 Published by Elsevier Ltd. All rights reserved.
doi:10.1016/j.optlaseng.2009.08.009

and phase composition had been investigated. Finally, the mechanical properties and fractured surface morphology had been analyzed. Mechanical properties of 304 stainless steel joints by TIG welding, laser welding and laser-TIG hybrid welding had been studied comparatively.

2. Experimental procedures

2.1. Welding process

In this experiment, A 5 kW Rofin TR050 CO_2 laser and a Miller 300A conventional DCEN TIG welder were used in the experiments. A welding head combined a CO_2 laser beam and a TIG torch was developed. This system was schematically shown in Fig. 1. The mode of the laser was TEM01. The laser beam was focused by mirror with the focal length 286.5 mm. The diameter of the focused laser beam was approximately 0.6 mm. The diameter of tungsten electrode was 2.4 mm, and distance between laser beam and tungsten electrode tip was 2.5 mm, while distance between plates and tungsten electrode tip was 3 mm in welding process.

The 3 mm thick 304 stainless steel plates were used as the welding materials. The composition (wt%) of material was Fe71.22–Cr18.66–Ni8.12–Mn1.14–Si0.75–C0.02. For concise description in this paper, the joint fabricated by TIG welding is denoted as J_T joint, while the joint fabricated by laser and hybrid welding are denoted as J_L and J_H joints, respectively. The surface of the plates was cleaned, degreased and dried before welding. The welding parameters are listed in Table 1. To observe the microstructure under the optical and electron microscope, specimens were cut from the welds, and then prepared according to the standard procedures. To study mechanical properties, the joints were sliced by abrasive cutters and then machined into the required dimensions to get tensile specimens. The fractured morphology of the specimens was analyzed by scanning electron microscopy (SEM). The joints were analyzed by a Philips X-ray diffractometer (XRD) for studying the phase composition.

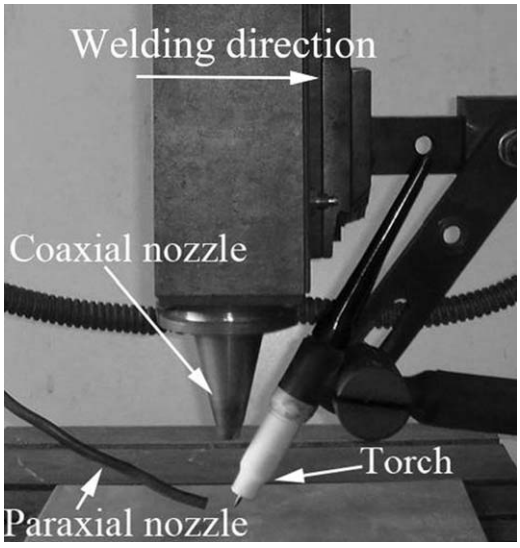

Fig. 1. Schematic setup of CO_2 laser-TIG hybrid welding.

Table 1
Welding parameters for experiments.

Specimens	TIG welding	Laser welding	Hybrid welding
Laser power (kW)	0	4	4
TIG current (A)	165	0	165
Welding speed (mm min^{-1})	400	1000	3000
TIG torch 50% He+50% Ar (L min^{-1})	15	0	15
Coaxial nozzle pure He (L min^{-1})	0	7.5	7.5
Paraxial nozzle pure Ar (L min^{-1})	0	7.5	0

3. Experimental results

3.1. Macrostructure and microstructure

Full penetration joints were produced by TIG welding, laser welding and laser-TIG hybrid welding. Macrostructure of the three joints is shown in Fig. 2. It can be seen that cracks and porosities cannot be found. For the three joints, the width and fusion area are different with each other. The width and fusion area of J_T joint are 6.6 and 13.9 mm^2, those of J_L joint are 3.5 and 6.7 mm^2. For the J_H joint, the width and fusion area are 4.2 and 7.2 mm^2, respectively. The width and fusion area of J_T joint are much larger than those of J_L and J_H joints. Different widths and fusion area are attributed to the different welding speed and heat-input used in the different welding methods.

The XRD analysis results of the three joints are given in Fig. 3. It can be demonstrated that δ-Fe phase and γ-Fe phase were found. In all the diffraction patterns, the diffraction peak of δ(110) in J_L joint has the highest intensity, while the diffraction peak of δ(110) in J_T joint has the lowest amount in all the three joints. It has been reported that the amount of δ-Fe in joints is a function of the thermal history experienced during welding. The higher the cooling rate, the higher δ-Fe content in joints [12]. The J_L and J_H joints share higher δ-Fe content than that in J_T joint.

Fig. 4 shows the optic micrograph near the weld junction of the three joints. The parent material and fusion zone could be discriminated easily in J_L and J_H joints. Columnar dendrites can be observed extending from the fusion boundary to the weld centerline. Moreover, there are no apparent transition zone and HAZ near the fusion boundaries in the two joints, while in the J_T joint, the transition zone and HAZ can be observed obviously. The width of the transition zone is approximate 70 μm. Fig. 5 shows the enlarged micrograph of J_T joint in the transition zone and HAZ. It can be seen that the δ-Fe exists as vermicular in transition zone (shown in Fig. 5a), while exists as skeletal in HAZ (shown in Fig. 5b) [13]. The average length and dendrite arm spacing of the δ-Fe in HAZ are about 80–140 and 10–30 μm, respectively.

Fig. 6 presents typical metallograph in fusion zone of the three joints. All joints are composed of dark δ-Fe dendritic structure in austenite matrix. However, different dendrite sizes can be observed in the three joints. The δ-Fe dendrite size in J_T joint is obviously larger than that in J_L and J_H joints. The primary and secondary dendrite arm spacing of J_T joint are about 10–14 and 3–7 μm, respectively. The J_L joint shows the smallest dendrite size in all joints. The primary dendrite arm spacing of J_L and J_H joint are about 2–5 and 4–8 μm, respectively. Furthermore, the δ-Fe in J_H joint exists as network morphology in fusion zone, while exists as columnar structure in J_L joint.

3.2. Mechanical properties

The transverse tensile strength of all joints had been evaluated. In each condition, three specimens have been tested and the average tensile strength of three results is obtained. The tensile strength of J_L joint is 733 MPa, while those of J_T and J_H joints are

560 and 683 MPa, respectively. The fractured surface of tensile specimens is analyzed using SEM.

Fig. 7 shows the SEM fractograph macrostructure of all joints. Different fracture mode can be observed obviously between the joints. Surface slip and necking down region can be observed from J_T joint, which is the typical characters of cup–cone shaped fracture, while for the J_L and J_H joints, it is just the pure-shear fracture mode, which results from the dislocation slip. Different micro-zones showed in Fig. 7 are investigated in detail to establish the nature of fracture.

The fractograph shows that relatively minor size dimples surround coarse dimples and a small quantity of tearing ridge (in Fig. 8) can be observed in J_T joint. There exists appreciable difference between J_T and J_L joints in the appearance of dimples. The J_L joint invariably consists of fine and uniform dimples (in Fig. 9), which indicate that the specimen fails in a ductile manner under the action of tensile loading. For the J_H joint, the fractograph consists of much smaller dimples, but some coarse dimples distribute sparsely among fine dimples [14] (in Fig. 10).

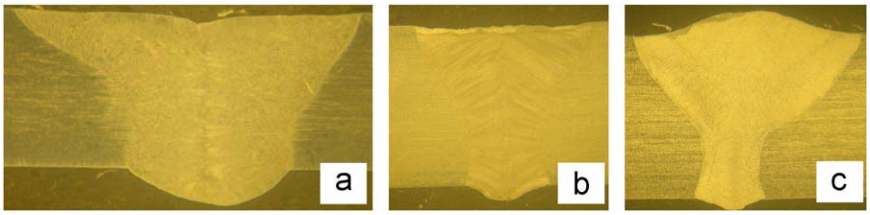

Fig. 2. Macrostructure of joints: (a) J_T joint, (b) J_L joint, (c) J_H joint.

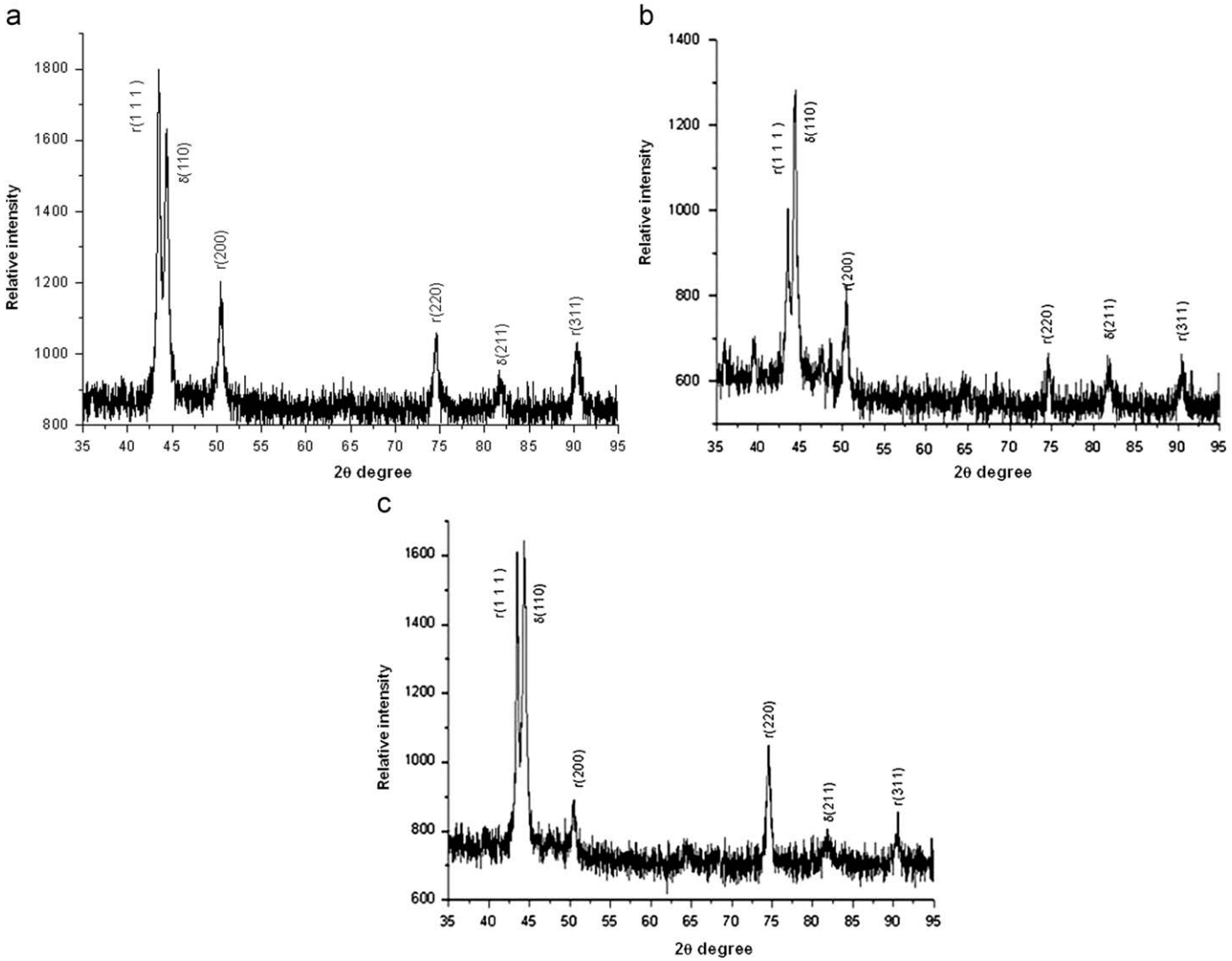

Fig. 3. XRD patterns of joints: (a) J_T joint, (b) J_L joint, (c) J_H joint.

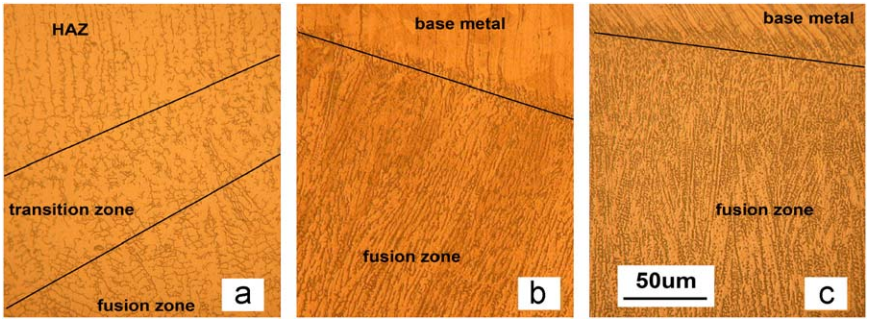

Fig. 4. Microstructure of joints: (a) J_T joint, (b) J_L joint (c) J_H joint.

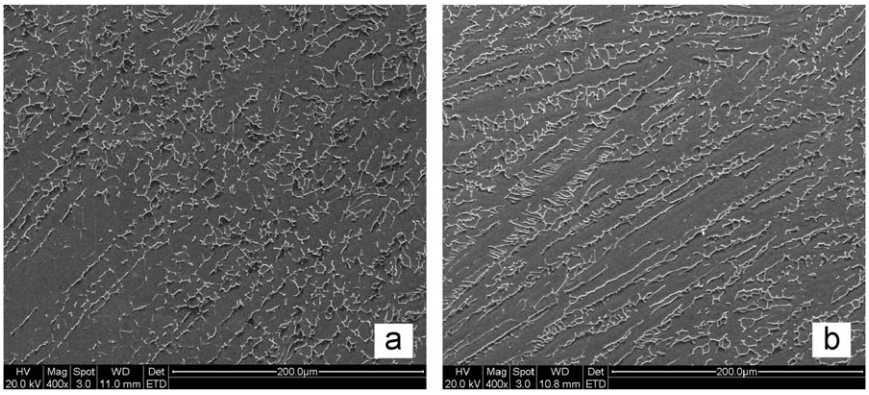

Fig. 5. Microstructure of J_T joint: (a) Vermicular morphology delta ferrite in transitional zone. (b) Skeletal morphology delta ferrite in HAZ.

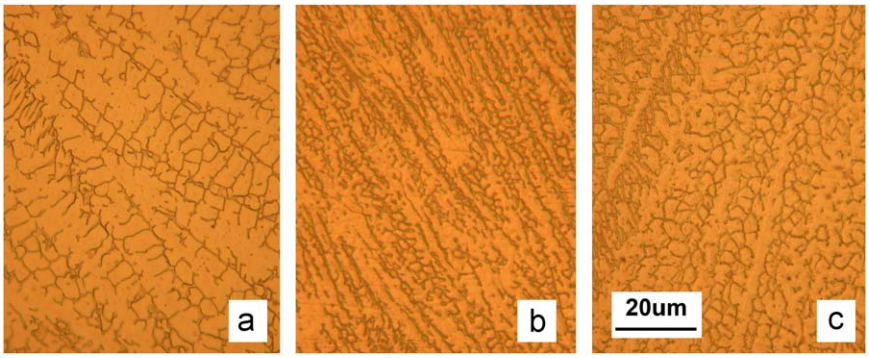

Fig. 6. Microstructure of joints: (a) J_T joint, (b) J_L joint, (c) J_H joint.

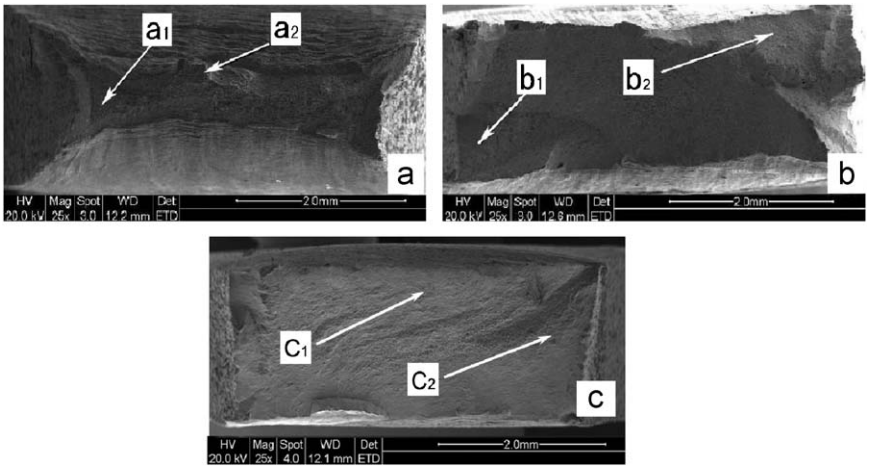

Fig. 7. SEM fractograph macrostructure of joints: (a) J_T joint, (b) J_L joint, (c) J_H joint.

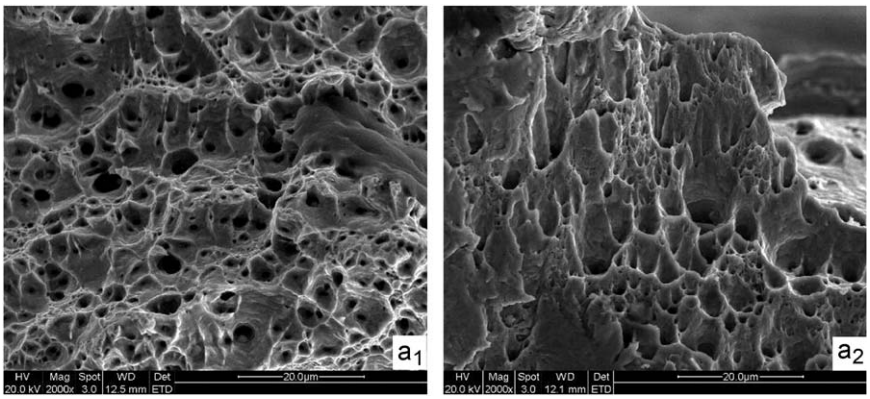

Fig. 8. SEM fractographs microstructure of J_T joint.

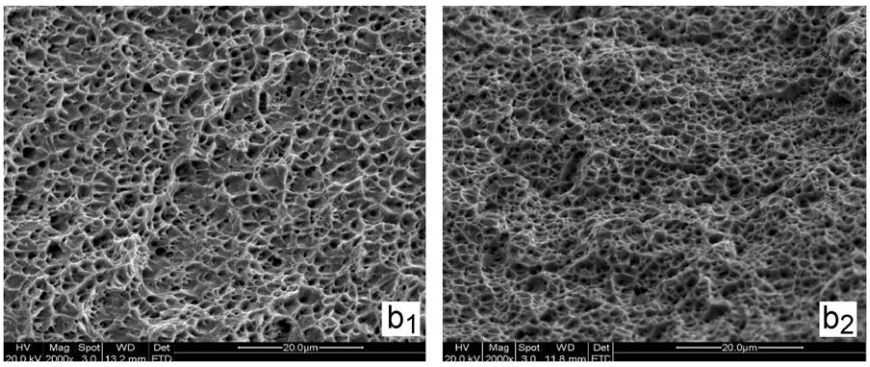

Fig. 9. SEM fractographs microstructure of J_L joint.

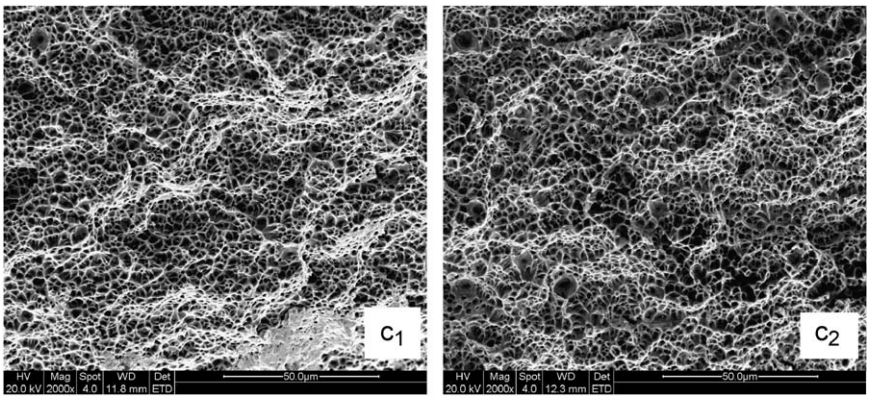

Fig. 10. SEM fractographs microstructure of J_H joint.

4. Discussion

Owing to the non-equilibrium rapid solidification condition in welding process, the peak temperature in fusion zone is much higher than the upper limit of phase balance between δ-Fe and γ-Fe phase. The austenite starts to precipitate at the ferrite grain boundaries during the cooling of joints in the temperature range 1573–1073 K [5]. Since the $\delta \rightarrow \gamma$ transformation is a diffusion-controlled process, the fast cooling in the welding process does not offer sufficient time to complete the phase transformation. As a result, a large portion of primary δ-Fe is retained in joints. Furthermore, the incomplete transformation results in the retention of skeletal δ-Fe dendritic within the austenite matrix.

The HAZ in J_T joint is attributed to the low welding speed and high heat-input used in the experiment. It causes to the fusion pool longer residence in high temperature zone and slower cooling rate, while for the J_L and J_H joints, higher welding speed and lower heat-input are adopted. The size of fusion pool is small and the cooling rate is very fast. During the cooling process, the gains between parent material and fusion zone have no time to grow up. Thus, the HAZ is absent in J_L and J_H joints and the absence HAZ in J_L and J_H joints is the reason of higher tensile strength when compared to J_T joint. Furthermore, high heat-input (and low cooling rate) was likely to induce the micro-segregation of alloying elements and formation of Cr-depleted zones, resulting in the degradation in mechanical properties for the

J_T joint [15–17]. Since the formation of the Cr carbides is caused by exposure to the temperature range of 773–1073 K, rapid cooling rate and shorter exposure time to the sensitization temperatures in J_L and J_H joints are preferable for prevention of sensitization and reduce the amount of Cr-rich carbides formed on the grain boundaries [18,19]. Therefore, a significant improvement in mechanical properties can be achieved in J_L and J_H joints when compared with J_T joint.

5. Conclusions

The following conclusions were derived from above experimental results and discussion.

Full penetration joints without any defects were produced by TIG welding, laser welding and laser-TIG hybrid welding. The microstructure of all joints is composed of δ-Fe phase and γ-Fe phases.

Transition zone and HAZ present in J_T joint obviously, while they are absent in J_H and J_L joints. The dendrite size in J_T joint is larger than that in J_L and J_H joints. The J_L joint shows the smallest dendrite size in all joints.

The tensile strength of J_T, J_L and J_H joints are 560, 733 and 683 Mpa, respectively. The J_T joint exists as cup–cone shaped fracture, while the J_L and J_H joints exist as pure-shear fracture.

The laser welding and hybrid welding are suitable for welding 304 stainless steel in industry application owing to high welding speed and excellent mechanical properties.

References

[1] Lee HT, Jeng SL. Characteristics of dissimilar welding of alloy 690 to 304L stainless steel. Sci Technol Weld Joining 2001;6(4):225–34.
[2] Jamshidi Aval H, Farzadi A, Serajzadeh S, Kokabi A.H. Theoretical and experimental study of microstructures and weld pool geometry during GTAW of 304 stainless steel. Int J Adv Manuf Technol 2008; doi:10.1007/s00170-008-1663-6.
[3] Lu SP, Fujii H, Nogi K, Sato T. Effect of oxygen content in He–O_2 shielding gas on weld shape in ultra deep penetration TIG. Sci Technol Weld Joining 2007;12(8):689–95.
[4] Lima AS, Nascimento AM, Abreu HFG, de Lima-Neto P. Sensitization evaluation of the austenitic stainless steel AISI 304L, 316L, 321 and 347. J Mater Sci 2005;40:143.
[5] Muthupandi V, Bala Srinivasan P, Seshadri SK, Sundaresan S. Effect of weld metal chemistry and heat input on the structure and properties of duplex stainless steel welds. Mater Sci Eng A 2003;358:9–16.
[6] Hu B., DenOuden G. Laser-assisted arc welding. Ph.D. Thesis. Delft University of Technology, 2002.
[7] Chen YB, Lei ZL, Li LQ, Wu L. Experimental study on welding characteristics of CO_2 laser TIG hybrid welding process. Sci Technol Weld Joining 2006;11(4):403–11.
[8] Decroix JH. Deformation Under Hot Working Conditions. The Iron and Steel Institute, London, 1968.
[9] Hanninen H, Romu J, Ilola R, Tervo J, Laitinen A. Effects of processing and manufacturing of high nitrogen-containing stainless steels on their mechanical, corrosion and wear properties. J Mater Process Technol 2001;117:424–30.
[10] Roberto Berretta Jose, de Rossi Wagner, Martins das Neves Mauricio David, de Almeida Ivan Alves, Vieira Junior Nilson Dias. Pulsed Nd:YAG laser welding of AISI 304 to AISI 420 stainless steels. Opt Laser Eng 2007;45:960–6.
[11] Anawa EM, Olabi AG. Optimization of tensile strength of ferritic/austenitic laser-welded components. Opt Laser Eng 2008;46:571–7.
[12] Capello E, Chiarello P, Previtali B, Vedani M. Laser welding and surface treatment of a 22Cr–5Ni–3Mo duplex stainless steel. Mater Sci Eng A 2003;351:334–43.
[13] Lee HT, Lin YD. Microstructure and corrosion behaviour of alloy 690–SUS 304L butt joints formed by electron beam welding. Sci Technol Weld Joining 2006;11(6):650–6.
[14] Magudeeswaran G, Balasubramanian V, Balasubramanian TS, Madhusudhan Reddy G. Effect of welding consumables on tensile and impact properties of shielded metal arc welded high strength, quenched and tempered steel joints. Sci Technol Weld Joining 2008;13(2):97–105.
[15] Patchett BM, Bringas J. The metals blue book, filler metals. CASTI Publishing Inc. and American Welding Society (AWS); 1998 p. 88.
[16] Folkhard E. Weld. Metall. Stainless Steel, 1988, p. 199.
[17] Ahlblom B, Sandstrom R. Int Met Rev 1982;1:1–27.
[18] Park Seung Hwan C, Sato Yutaka S, Kokawa Hiroyuki, Okamoto Kazutaka, Hirano Satoshi, Inagaki Masahisa. Corrosion resistance of friction stir welded 304 stainless steel. Scr Materialia 2004;51:101–5.
[19] McPherson NA, Li Y, Baker TN. Microstructure and properties of as welded duplex stainless steel. Sci Technol Weld Joining 2000;5(4):235–44.